

Transverse-Leaky-Mode Characteristics of ARROW VCSELs

C. W. Tee, *Student Member, IEEE*, S. F. Yu, *Senior Member, IEEE*, and N. S. Chen

Abstract—Transverse-leaky-mode characteristics of antiresonant-reflecting-optical-waveguide (ARROW) vertical-cavity surface-emitting lasers (VCSELs) are studied. It is found that the suppression of high-order transverse leaky modes in ARROW VCSELs can be deteriorated by the influence of spatial hole burning and thermal lensing effects. On the other hand, a new design rule is proposed to deduce the optimum dimensions of ARROW so that the suppression of high-order transverse leaky modes can be enhanced. Furthermore, the turn-on transient response of ARROW VCSELs is investigated. It is found that the radiation loss has significant influence on the built-up time of the first-order transverse leaky mode.

Index Terms—Antiresonant reflecting optical waveguide (ARROW), mode control, multitransverse mode, semiconductor laser modeling, spatial hole burning (SHB), thermal lensing effect, vertical-cavity surface-emitting lasers (VCSELs).

I. INTRODUCTION

RECENTLY, extensive studies have been concentrated on the modal characteristics of antiresonant-reflecting optical waveguides (ARROWs). It is shown that the radiation loss of the fundamental transverse leaky mode can be very small, while the radiation losses of the high-order transverse leaky modes remained fairly large. This is because of the antiresonant characteristics of ARROW [1]–[3]. Hence, ARROW structures are employed to suppress the excitation of high-order transverse leaky modes in vertical-cavity surface-emitting lasers (VCSELs), especially for those with a large core diameter [4]. However, it is observed from experiments that high-order transverse leaky modes can still be excited in ARROW VCSELs under pulsed and continuous-wave (CW) operation [4]. This implies that the cold-cavity simulations [3]–[5] have underestimated the influence of spatial hole burning (SHB) and thermal lensing effects on the excitation of high-order transverse modes. On the other hand, the available above-threshold models of multimode ARROW lasers, in which only the effects of the current injection profile and SHB-induced focusing/defocusing are taken into consideration, were developed for planar structures [6], [7]. However, a self-consistent electro-opto-thermal model for multimode cylindrical ARROW VCSELs is lacking. Therefore, it is necessary to develop a more exact above-threshold model to investigate the multi-leaky-mode characteristics of ARROW VCSELs.

In the design of ARROW VCSELs, the dimension of the ARROW is often selected to minimize the radiation loss of the fundamental transverse leaky mode [4]. This is because if the radiation loss can be minimized in ARROW VCSELs, the corresponding threshold current (output power) can be further decreased (increased). However, the large radiation loss margin between the fundamental and first-order transverse leaky modes may not be guaranteed for this design consideration [5]. As a result, high-order transverse leaky modes in ARROW VCSELs with a large core diameter can still be excited by SHB and thermal lensing effects. Therefore, it is necessary to deduce a different design rule to calculate the optimum dimension of ARROW for better suppression of high-order transverse leaky modes.

In gain- or index-guided VCSELs, the turn-on transient response of the transverse modes is mainly affected by SHB through the time variation of modal gain. However, the transient competition of leaky modes in ARROW VCSELs is dependent on the balance between modal gain and radiation loss. Hence, the turn-on transient response of ARROW VCSELs can be different to that of gain- or index-guided VCSELs. If the multimode characteristics of ARROW VCSELs are to be used as the light sources of high-speed multimode data links [8], it is necessary to investigate the turn-on transient response of ARROW VCSELs.

In this paper, a self-consistent model, with SHB of carrier concentration and thermal lensing effects taken into consideration, is developed to analyze the above-threshold characteristics of ARROW VCSELs [9]. Exact calculation of transverse leaky modes inside the cylindrical ARROW is also performed. Hence, the steady-state characteristics of ARROW VCSELs obtained from the experiments [4] can be explained. Furthermore, a new design rule is proposed to deduce the optimum dimension of the cylindrical ARROW so that the suppression of high-order transverse leaky modes can be enhanced in large-aperture ARROW VCSELs. The turn-on transient response of ARROW VCSELs is also investigated. It can be shown that the long built-up time of the first-order transverse leaky mode is due to the presence of radiation loss.

II. MODEL

Fig. 1 shows the schematic of an ARROW VCSEL used in our analysis. The low-index core region (with diameter d_1) is surrounded by two reflectors, which are the first and second cladding layers, with a thickness of s and d_2 , respectively. It must be noted that the high-order transverse leaky modes experience high radiation losses due to the antiresonant characteristics of the ARROW. Therefore, only the two lowest radi-

Manuscript received September 30, 2003; revised February 11, 2004.

The authors are with the School of Electrical and Electronic Engineering, Nanyang Technological University, Singapore 639798, Singapore (e-mail: esfyu@ntu.edu.sg).

Digital Object Identifier 10.1109/JLT.2004.831091

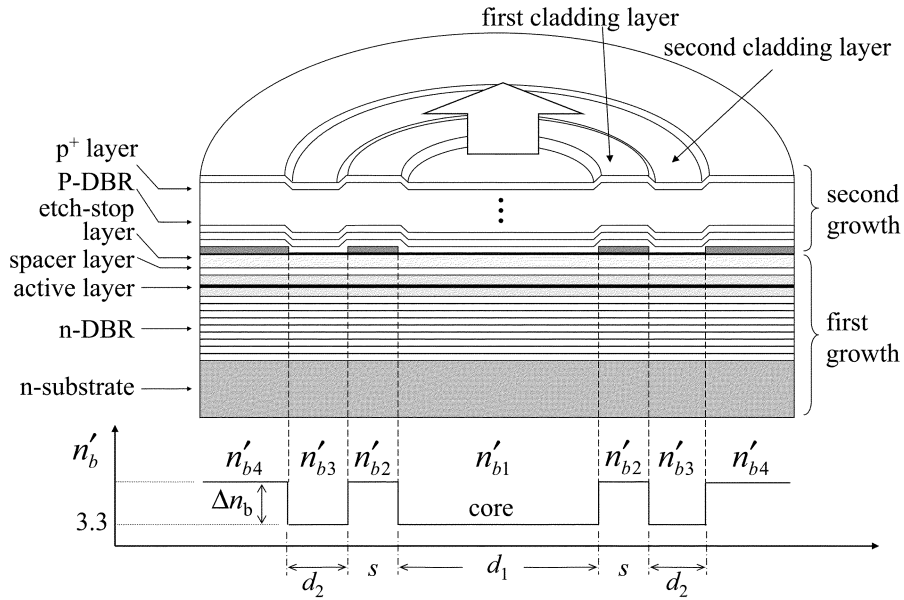


Fig. 1. Schematic of an ARROW VCSEL.

tion losses transverse leaky modes (i.e., LM_{01} and LM_{11} , where LM stands for leaky modes) are required to be considered in the investigation. Furthermore, due to the axis-symmetric geometry of the device, the azimuthal degree of freedom of the transverse leaky modes has to be taken into account. This can be done by attributing each LM_{m1} mode (where $m = 0$ or 1) a cosine (LM_{m1}^c) and sine (LM_{m1}^s) azimuthal dependence [10]. The transverse field ψ_{m1}^i and the transverse propagation coefficient β_{m1}^i can be calculated from the scalar Helmholtz equation as shown in the following:

$$\left(\frac{1}{r} \frac{\partial}{\partial r} \left(r \frac{\partial}{\partial r} \right) + \frac{1}{r^2} \frac{\partial^2}{\partial \phi^2} + n_0^2 k_o^2 - (\beta_{m1}^i)^2 \right) \psi_{m1}^i = 0 \quad (1)$$

where $i = c$ or s , n_0 is the refractive index profile of the ARROW, $k_o (= 2\pi/\lambda)$ is the wave vector, and $\lambda (= 0.98 \mu\text{m})$ is the free-space wavelength. If the refractive index of the ARROW along the azimuthal direction ϕ is assumed to be uniform, the profile of the transverse field with cosine and sine azimuthal dependence ψ_{m1}^c and ψ_{m1}^s can be expressed as [11]

$$\psi_{m1}^c = \left(E^+ H_v^{(1)}(\beta_{m1}^c r) + E^- H_v^{(2)}(\beta_{m1}^c r) \right) \cos(\phi) \quad (2)$$

$$\psi_{m1}^s = \left(E^+ H_v^{(1)}(\beta_{m1}^s r) + E^- H_v^{(2)}(\beta_{m1}^s r) \right) \sin(\phi) \quad (3)$$

where E^+ (E^-) is the positive (negative) traveling field amplitude along the transverse direction, and $H_v^{(1)}$ ($H_v^{(2)}$) is the v th-order Hankel function of the first (second) kind. It must be noted that in the absence of SHB and thermal lensing effects, $n_0 = n'_b$, where n'_b is the built-in refractive-index profile of the ARROW. However, due to the influence of SHB and thermal lensing effects, n_0 has to be rewritten as $n_0^2 = n_b^2(r) + \Delta\epsilon(r, \phi)$, where n_b is the variation of the built-in refractive-index profile and $\Delta\epsilon$ is a small perturbation of material permittivity along the transverse and azimuthal directions. The small variation of

ψ_{m1}^i , $\Delta\psi_{m1}^i$ and that of β_{m1}^i , $\Delta\beta_{m1}^i$ can be estimated by the first-order perturbation method [12]

$$\begin{aligned} \Delta\psi_{m1}^i &= \frac{1}{\int_0^{2\pi} \int_0^\infty |\psi_{m1}^i(r, \phi)|^2 r dr d\phi} \\ &\times \sum_{n \neq m} \frac{k_o^2 \int_0^{2\pi} \int_0^\infty \psi_{n1}^{i*}(r, \phi) \Delta\epsilon(r, \phi) \psi_{m1}^i(r, \phi) r dr d\phi}{\beta_{m1}^{i2} - \beta_{n1}^{i2}} \\ &\times \psi_{n1}^i(r, \phi) \end{aligned} \quad (4)$$

$$\begin{aligned} \Delta\beta_{m1}^i &= \frac{k_o^2 \int_0^{2\pi} \int_0^\infty \psi_{m1}^{i*}(r, \phi) \Delta\epsilon(r, \phi) \psi_{m1}^i(r, \phi) r dr d\phi}{2\beta_{m1}^i \int_0^{2\pi} \int_0^\infty |\psi_{m1}^i(r, \phi)|^2 r dr d\phi} \end{aligned} \quad (5)$$

where the superscript “*” represents the complex conjugate. Hence, the resultant transverse field ψ_{m1}^i and transverse propagation coefficient β_{m1}^i can be written as $\psi_{m1}^i = \psi_{m1}^i + \Delta\psi_{m1}^i$ and $\beta_{m1}^i = \beta_{m1}^i + \Delta\beta_{m1}^i$, respectively.

The photon rate equations that describe the competition of the transverse modes inside an ARROW VCSEL can be written as [13]

$$\frac{dS_{m1}^i}{dt} = \nu_g (\Gamma_z \langle g_{m1}^i \rangle - \alpha_{m1}^i - \zeta_{m1}^i) S_{m1}^i + \beta_{sp} \Gamma_z B_{sp} \langle N \rangle^2 \quad (6)$$

where S_{m1}^i is the photon density of LM_{m1}^i , $\Gamma_z (= 0.06)$ is the confinement factor along the longitudinal direction, $\nu_g (= 83.3 \times 10^8 \text{ cm/s})$ is the group velocity, $B_{sp} (= 1 \times 10^{-10} \text{ cm}^3/\text{s})$ is the biomolecular recombination coefficient, $\beta_{sp} (= 1 \times 10^{-5})$ is the spontaneous emission factor, and $\alpha_{m1}^i (= 2 \times \text{Im}(\beta_{m1}^i)/k_o)$ is the radiation loss. In (6), it is assumed that the polarization mechanism of the ARROW VCSEL is mainly dependent on the polarization and gain/loss

anisotropies inside the laser cavity, so the influence of carrier spin effects [14] is ignored in the calculation. The modal gain $\langle g_{m1}^i \rangle$ is given by

$$\langle g_{m1}^i \rangle = \frac{\int_0^{2\pi} \int_0^\infty g(N) |\psi_{m1}^i(r, \phi, t)|^2 r dr d\phi}{\int_0^{2\pi} \int_0^\infty |\psi_{m1}^i(r, \phi, t)|^2 r dr d\phi} \quad (7)$$

where $g(N) = a_N \log [N(r, \phi, t)/N_t]$, N is the carrier concentration, $N_t (= 1.5 \times 10^{18} \text{ cm}^{-3})$ is the transparent carrier density, and $a_N (= 1.5 \times 10^3 \text{ cm}^{-1})$ is the gain coefficient. $\langle N \rangle$ in (6) has the similar definition as $\langle g_{m1}^i \rangle$. The values of the total cavity loss $\zeta_{m1}^{c,s}$ (including mirror and absorption losses) of LM₀₁ and LM₁₁ are given by

$$\zeta_{m1}^{c,s} = \begin{cases} 50 \text{ cm}^{-1} & m = 0 \\ 65 \text{ cm}^{-1} & m = 1 \end{cases}. \quad (8)$$

In (8), it is assumed that LM₁₁ has higher cavity loss than that of LM₀₁. This is because LM₁₁ has a large portion of the field-intensity residing inside the cladding region with high absorption loss due to ion implantation. The output power of the ARROW VCSEL is calculated by $P_{m1}^i = hf v_g (1 - r_{\text{eff}}^2) A S_{m1}^i$, where h is the Planck's constant, f is the lasing frequency, $r_{\text{eff}} (= 0.99847)$ is the effective reflectivity of the Bragg reflectors, and $A (= \pi d_1^2/4)$ is the area of core region.

The rate equation that accounts for the transverse and azimuthal variation of carrier concentration $N(r, \phi, t)$ is given by

$$\frac{\partial N}{\partial t} = D \left[\frac{1}{r} \frac{\partial N}{\partial r} + \frac{\partial^2 N}{\partial r^2} \right] + D \frac{1}{r^2} \frac{\partial^2 N}{\partial \phi^2} + \frac{J(r, t)}{qd} - \frac{N}{\tau_N} - v_g \sum_{\substack{m=0,1 \\ i=c,s}} g(N) |\psi_{m1}^i|^2 S_{m1}^i \quad (9)$$

where $D (= 1 \text{ cm}^2/\text{s})$ is the diffusion coefficient, $q (= 1.602 \times 10^{-19} \text{ C})$ is the electron charge, $d (= 0.1 \times 10^{-4} \text{ cm})$ is the thickness of active layer, and $\tau_N (= 1 \text{ ns})$ is the carrier lifetime. If current is injected into the core region through a transparent electrode with the same diameter as the core region, then the injection current density $J(r, t)$ can be expressed as [15]

$$J(r, t) = \begin{cases} J_e(t), & r \leq \frac{d_1}{2} \\ J_e(t) \exp\left(\frac{-(r - \frac{d_1}{2})}{r_o}\right), & r > \frac{d_1}{2} \end{cases} \quad (10)$$

where J_e denotes the current density at the edge and within the contact area ($r \leq d_1/2$) and $r_o (= 1.5 \text{ } \mu\text{m})$ is the effective diffusion length of the injection current. The carrier rate (9) can be solved rigorously by the two-dimensional finite-difference method, but with the expense of extensive computational time. Therefore, a simple perturbation method is adopted to improve the computational speed of the model [10]. This can be done by expanding the carrier concentration in a series expansion as shown in the following:

$$N(r, \phi, t) = \sum_{k=0}^{\infty} [N_{ck}(r, t) \cos(k\phi) + N_{sk}(r, t) \sin(k\phi)]. \quad (11)$$

By substituting (11) into (9) and integrating over ϕ , one obtains

$$\begin{aligned} \frac{\partial N_{c0}}{\partial t} = & D \left[\frac{1}{r} \frac{\partial N_{c0}}{\partial r} + \frac{\partial^2 N_{c0}}{\partial r^2} \right] - \frac{N_{c0}}{\tau_N} + \frac{J(r, t)}{qd} \\ & - v_g \langle g_{01}^c \rangle |\psi_{01}^c(r)|^2 S_{01}^c - v_g \langle g_{11}^c \rangle |\psi_{11}^c(r)|^2 S_{11}^c \\ & - v_g \langle g_{01}^s \rangle |\psi_{01}^s(r)|^2 S_{01}^s - v_g \langle g_{11}^s \rangle |\psi_{11}^s(r)|^2 S_{11}^s \end{aligned} \quad (12)$$

where N_{c0} is the transverse distribution of carrier concentration. Again, substituting (11) into (9) and multiplying $\cos(2\phi)$ before integrating over ϕ gives

$$\begin{aligned} \frac{\partial N_{c2}}{\partial t} = & D \left[\frac{1}{r} \frac{\partial N_{c2}}{\partial r} + \frac{\partial^2 N_{c2}}{\partial r^2} \right] - D \frac{4}{r^2} N_{c2} - \frac{N_{c2}}{\tau_N} \\ & - \frac{1}{2} v_g \langle g_{11}^c \rangle |\psi_{11}^c(r)|^2 S_{11}^c - \frac{1}{2} v_g \langle g_{11}^s \rangle |\psi_{11}^s(r)|^2 S_{11}^s \end{aligned} \quad (13)$$

where N_{c2} is the equivalent transverse perturbation of carrier concentration due to the azimuthal variation of transverse fields. The required boundary conditions to solve (12) are $\partial N_{c0}(0, \phi, t)/\partial r = 0$ and $N_{c0}(\infty, \phi, t) = 0$, and that to solve (13) are $N_{c2}(0, \phi, t) = 0$ and $N_{c2}(\infty, \phi, t) = 0$.

It must be noted that the change of N_{c0} and N_{c2} will induce the variation of refractive index inside the active layer along the radial and azimuthal directions. The variation of refractive index along the r direction, $\delta n_0(r)$ can be expressed as

$$\delta n_0(r, t) = -\alpha_H \frac{\lambda}{4\pi} \Gamma_z \frac{a_N}{N_{c0}} \Delta N_{c0}(r, t) \quad (14)$$

where $\alpha_H (= 3)$ is the linewidth enhancement factor and ΔN_{c0} is the change of carrier concentration N_{c0} . Hence, using $n_b = n'_b + \delta n_0$, the variation of $\psi_{m1}^i(r)$ and $\beta_{m1}^i(r)$ due to ΔN_{c0} can be deduced from (1). Apart from that, the variation of refractive index along ϕ due to the change in N_{c2} (i.e., ΔN_{c2}) can also be taken into consideration by approximating the variation of permittivity $\Delta \varepsilon$ as

$$\Delta \varepsilon(r, \phi, t) \cong 2n_b(r, t) \cdot \delta n_2(r, \phi, t) \quad (15)$$

where

$$\delta n_2(r, \phi, t) = -\alpha_H \frac{\lambda}{4\pi} \Gamma_z \frac{a_N}{N_{c2}} \Delta N_{c2} \cos(\phi). \quad (16)$$

Hence, substituting (15) into (4) and (5), the dependence of $\Delta \psi_{m1}^i$ and $\Delta \beta_{m1}^i$ on the variation of refractive index along azimuthal direction can also be introduced into our calculation.

Furthermore, thermal lensing effects can be included into the model by solving the heat conduction equation using Green's function methods [16]. The variation of temperature along the active layer $T(r, t)$ can be written as

$$T(r, t) = T_0 + \frac{4}{HW^2} \sum_{m=1}^{\infty} \sum_{n=1}^{\infty} \frac{A_{mn}}{J_0^2(L_n W)} \sin(K_m z_a) J_0(L_n r) \quad (17)$$

where T_0 is the background temperature, z_a is the distance between the heat sink and active layer, H is the height of the VCSELS, $W = d_1/2 + s + d_2$, J_0 is the zeroth-order Bessel function of the first kind, and see (18), shown at the bottom of

the page, where $Q(r, z)$ is the heat density, λ_i is the thermal conductivity, k_i is the thermal diffusivity, and η_m are the roots of $J_1(L_n w) = 0$. In addition, $K_m = (2m - 1)/2W$ and $L_n = \eta_m/d_1$ where m and n are integers. It must be noted that the injection current density J is independent of ϕ . Therefore, it is reasonable to assume that $T(r, t)$ is uniformly distributed over the ϕ direction. Thermal-induced refractive-index variation δn_T inside the active layer can then be expressed in term of the temperature change as $\delta n_T(r, t) = (\partial n / \partial T) \Delta T(r, t)$, where $\partial n / \partial T (\sim 3 \times 10^{-4} \text{ K}^{-1})$ is the heat-induced index change and $\Delta T = T - T_0$. Hence, the influence of thermal lensing effects on the variation of ψ_{m1}^i and β_{m1}^i can be calculated by (1) using $n_b = n'_b + \delta n_0 + \delta n_T$. For information on the parameters used to solve (17), please refer to [17]. Note that the temperature dependency of the parameters a_N , N_t , and τ_N has been ignored in order to facilitate our study. Therefore, thermal rollover of the light-current curve is not included in our model. This approximation is still valid because the excitation of high-order transverse modes is mainly dependent on the refractive index profile inside the active layer.

III. NUMERICAL SIMULATION

In the following sections, the steady-state characteristics of ARROW VCSELs are studied. A new design rule is proposed to suppress the excitation of high-order transverse leaky modes in large-core-diameter ARROW VCSELs, especially for those under CW operation. The dynamic responses are also studied.

A. Steady-State Above-Threshold Analysis of ARROW VCSELs

The steady-state characteristics of ARROW VCSELs with dimensions that are the same as that reported in [4] are studied. In the calculation, d_1 , s , and d_2 are set to 12, 2.4, and 6 μm , respectively. The built-in index step Δn_b is set to 0.05, with $n'_{b1} = n'_{b3} = 3.3$ and $n'_{b2} = n'_{b4} = 3.3 + \Delta n_b$. Other parameters used in the calculation can be found in Section II. The steady-state characteristics of the ARROW VCSEL are investigated through the study of light-current (L - I) curve, gain margin, radiation loss margin, and side-mode suppression ratio. The gain margin (GM) is defined as $\text{GM} = (1/2) \sum_{i=c,s} \{ (\langle g_{01}^i \rangle - \alpha_{01}^i - \zeta_{01}^i) - (\langle g_{11}^i \rangle - \alpha_{11}^i - \zeta_{11}^i) \}$, which measures the difference in modal gains between the fundamental and first-order transverse modes. The radiation loss margin (RLM) is defined as $\text{RLM} = -(1/2) \sum_{i=s,c} (\alpha_{01}^i - \alpha_{11}^i)$, which indicates the differences in radiation losses between the fundamental and first-order transverse modes. The side-mode suppression ratio (SMSR) is given by $\text{SMSR} = 10 \log_{10} \{ (P_{01}^s + P_{01}^c) / (P_{11}^s + P_{11}^c) \}$. Fig. 2 shows the calculated (a) L - I curve, (b) GM, (c) RLM, and (d) SMSR of the ARROW VCSEL. In the figures, the dashed-dotted and solid lines represent the cases with and without thermal lensing effects taken into consideration, re-

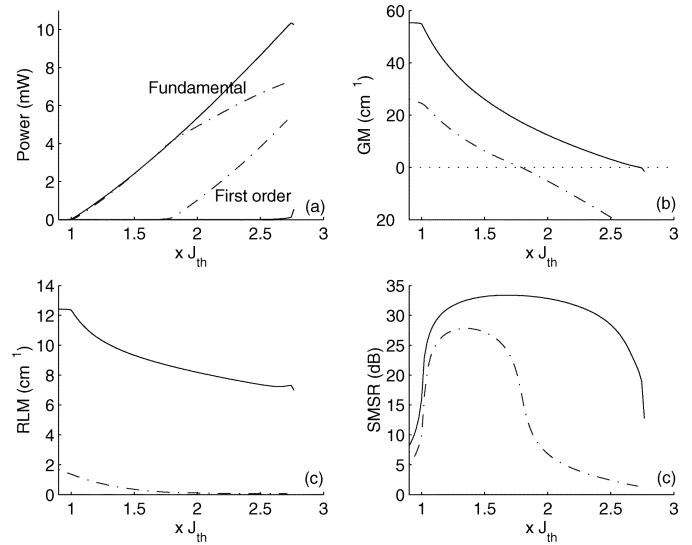


Fig. 2. Steady-state characteristics of a 12- μm -core-diameter ARROW VCSEL. (a) L - I curve, (b) GM, (c) RLM, and (d) SMSR.

spectively. It is observed that for the case where only the SHB of carrier concentration is considered, VCSEL shows single-mode emission for the injection level up to $\sim 2.8 \times$ threshold, which corresponds to an output power of ~ 10 mW. However, with the inclusion of thermal lensing effects, ARROW VCSEL exhibits multimode operation for the injection level $> 1.8 \times$ threshold, with a maximum single-mode output power of ~ 4.5 mW. It is observed that the L - I curve given in Fig. 2(a) agrees quantitatively with the experimental results reported in [4]. The corresponding values of GM and RLM reduce over 30 and 10 cm^{-1} , respectively, under the influence of thermal lensing effects. In addition, SMSR reduces by 10 dB at a small injection level and decreases more than 20 dB when side mode is excited.

In order to investigate the excitation mechanism of high-order transverse leaky modes in 12- μm -core-diameter ARROW VCSELs under CW operation, Fig. 3 plots the (a) LM_{01} field intensity, (b) LM_{11} field intensity, (c) refractive-index profile $\delta n_0 + \delta n_T$, (d) N_{c0} , (e) N_{c2} , and (f) heat profile ΔT versus r for injection current equal to 0.8, 1, 1.25, 1.5, 1.8, 2.25 \times threshold. From Fig. 3(a) and (b), it is observed that the increase in injection current causes the focusing of the fundamental and first-order transverse leaky modes toward the center. As a result, the modal gain (radiation loss) of the first-order transverse mode is greatly enhanced (reduced), causing the onset of multimode operation at a high injection level. The focusing of transverse leaky modes is due to the increase in refractive index inside the core region. The variation of the refractive-index profile along the core region can be attributed to the nonuniform distribution of carrier concentration and heat. However, it is observed from Fig. 3(c)-(f) that the profile of the refractive index

$$A_{mn} = \int_0^t \int_0^H \int_0^W \frac{k_i}{\lambda_i} \sin(K_m z) J_0(L_n r) r Q(r, z) \times \exp[k_i(K_m^2 + L_n^2)(u - t)] dudrdz \quad (18)$$

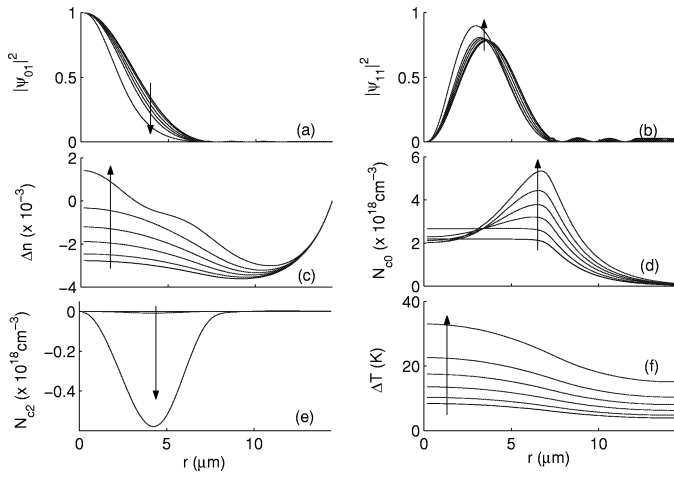


Fig. 3. Steady-state characteristics of a 12- μm -core-diameter ARROW VCSEL. (a) Field-intensity profile of LM_{01}^i , (b) field-intensity profile of LM_{11}^i , (c) transverse refractive-index change, (d) N_{e0} ($\times 10^{18} \text{ cm}^{-3}$), (e) N_{e2} ($\times 10^{18} \text{ cm}^{-3}$), and (f) temperature rise along the transverse direction in active region (K). The arrows indicate the change in profiles with the increase of injection current.

closely follows the heat distribution. Therefore, it is shown that the effect of thermal lensing dominates over the SHB of carrier concentration.

B. New Design Rule for ARROW VCSELS

In the design of ARROW VCSELS, dimensions of the cladding layers are often selected such that the radiation loss of the fundamental transverse leaky mode is minimum. However, this design consideration does not necessarily guarantee a large RLM. As a result, excitation of high-order transverse leaky modes will occur in ARROW VCSELS due to the influence of SHB and thermal lensing effects. Therefore, a new design rule is proposed to improve the above-threshold performance of ARROW VCSELS. The design rule can be explained as follows: for a given core diameter d_1 , the dimensions of the cladding layers s and d_2 of the ARROW are selected to minimize the radiation loss of the fundamental transverse leaky mode. Then, the value of s is varied to achieve higher RLM, while at the same time keeping the radiation loss of the fundamental transverse leaky mode at a reasonably small value. In essence, the proposed method sought to maximize the radiation loss margin between the fundamental mode and the next lowest loss mode. The procedures to implement the design rule can be illustrated by the design of a 12- μm -core-diameter ARROW VCSEL. It can be shown that the values of s and d_2 for minimum radiation loss ($\sim 0.079 \text{ cm}^{-1}$) of the fundamental transverse leaky mode are $\sim 1.28 \mu\text{m}$ and $3.9 \mu\text{m}$, respectively [5].

Fig. 4 plots the radiation losses of the four lowest radiation loss transverse modes against s for $d_1 = 12 \mu\text{m}$, $d_2 = 3.9 \mu\text{m}$, and $\Delta n_b = 0.05$. It is noted that when $s = 2.46 \mu\text{m}$, the new RLM is $\sim 14 \text{ cm}^{-1}$, and the radiation loss of the fundamental leaky mode is $\sim 0.45 \text{ cm}^{-1}$. If the value of s is further increased at this point, the fundamental leaky mode will be resonating in the first cladding layer and the corresponding radiation loss will increase to 4 cm^{-1} .

In Fig. 5, the field-intensity profile of the four leaky modes is also plotted with $s = 2.46 \mu\text{m}$. This new design rule can

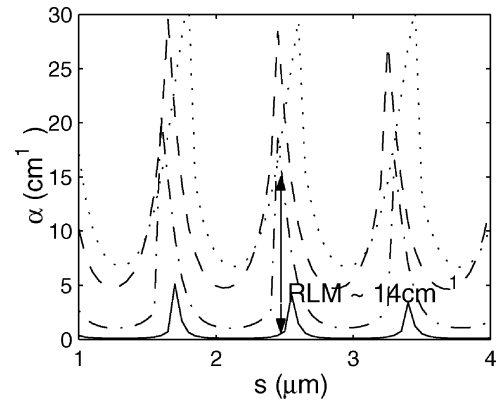


Fig. 4. Radiation loss of the four lowest loss leaky modes plotted against the first cladding layer s with $d_1 = 12 \mu\text{m}$ and $d_2 = 3.9 \mu\text{m}$. The four leaky modes LM_{01}^i , LM_{11}^i , LM_{02}^i , and LM_{12}^i are labeled as fundamental (solid line), first (dashed-dotted line), second (dotted line), and third (dashed line) order, respectively.

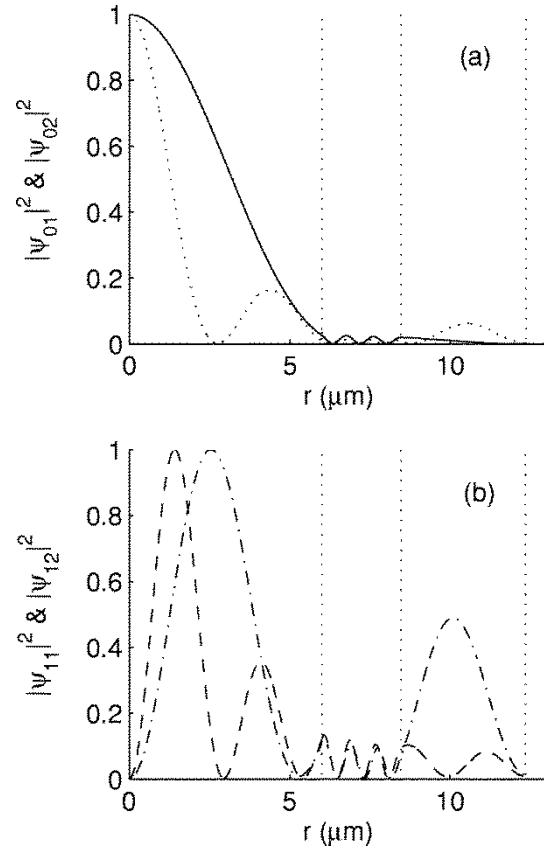


Fig. 5. Field-intensity profile of leaky modes (a) LM_{01} (solid line) and LM_{02} (dotted line) and (b) LM_{11} (dashed-dotted line) and LM_{12} (dashed line), with $d_1 = 12 \mu\text{m}$, $s = 2.46 \mu\text{m}$, and $d_2 = 3.9 \mu\text{m}$.

be used to evaluate the optimum dimensions of the ARROW for single-mode emission because the RLM is maximized but the radiation loss of the fundamental mode is only slightly increased. This enhancement of RLM can be explained by the field-intensity profile of the first-order transverse leaky mode.

Fig. 6 plots the field-intensity profile of the first-order transverse mode using (a) $s = 2.4 \mu\text{m}$ and $d_2 = 6 \mu\text{m}$ and (b) $s = 2.46 \mu\text{m}$ and $d_2 = 3.9 \mu\text{m}$. It is noted that in Fig. 6(b), the first-order transverse mode experiences a much higher radiation

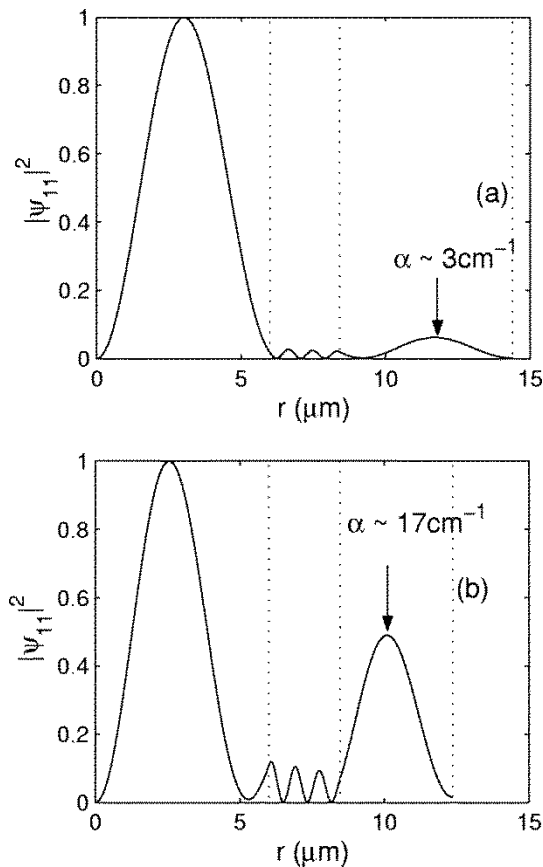


Fig. 6. (a) Field-intensity profile of the first-order mode (LM_{11}^i) in conventional ARROW VCSEL. (b) Field-intensity profile of the first-order mode in ARROW VCSEL designed based on the new approach.

loss. This is because a large portion of the first-order transverse leaky mode is distributed within the second cladding layer (beyond the current confinement region). As a result, RLM is improved in the new design as the corresponding first-order transverse leaky mode suffers a much higher absorption loss than that of the conventional design.

Fig. 7 compares the performance of the two design methods of ARROW VCSEL in terms of (a) the L - I curve and (b) the SMSR. In the figure, the solid line (dashed-dotted line) denotes device designed using the new approach (conventional approach). It is observed that the new design is capable of delaying the onset of first-order transverse leaky mode from 1.8 to $2.3 \times$ threshold. Furthermore, the maximum single-mode power is improved from ~ 4 to ~ 7 mW (i.e., more than 75% of improvement). SMSR is also increased by more than ~ 6 dB under a low injection current when compared with the conventional design.

Fig. 8(a) plots the radiation losses of the four transverse leaky modes (LM_{01}^i , LM_{11}^i , LM_{02}^i , and LM_{12}^i) versus s for $d_1 = 12 \mu\text{m}$, $d_2 = 6 \mu\text{m}$, and $\Delta n_b = 0.05$ using the matrix method [11]. It is found that the radiation loss of the fundamental mode and the corresponding RLM are equal to ~ 0.385 and $\sim 3 \text{ cm}^{-1}$, respectively, if $s = 2.4 \mu\text{m}$ is used instead of the value for minimum radiation loss of the fundamental transverse leaky mode. On the other hand, the variation of radiation losses of the $8\text{-}\mu\text{m}$ -core-diameter ARROW VCSEL with $d_2 = 4 \mu\text{m}$ and $\Delta n_b = 0.05$ is plotted versus s in Fig. 8(b).

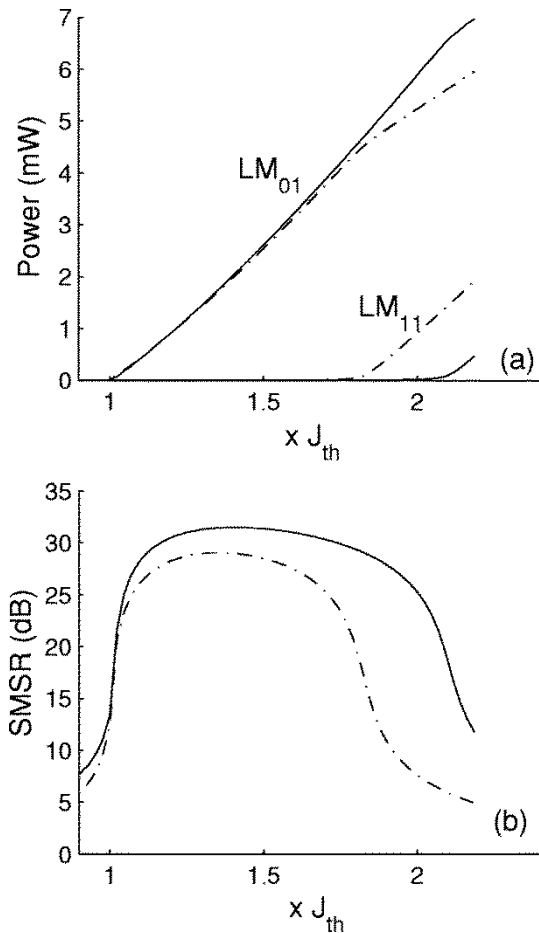


Fig. 7. (a) L - I curve and (b) side-mode suppression ratio for ARROW VCSEL designed using different approach.

In this case, the radiation loss of the fundamental mode and the corresponding RLM are found to be ~ 2 and $\sim 13 \text{ cm}^{-1}$, respectively, when $s = 2.4 \mu\text{m}$. It is observed that the RLM of the $12\text{-}\mu\text{m}$ and $8\text{-}\mu\text{m}$ ARROW VCSELs has been improved from 1 to 3 cm^{-1} and 7 to 13 cm^{-1} , respectively. Note that the RLM value of the $12\text{-}\mu\text{m}$ device is relatively smaller than that of the $8\text{-}\mu\text{m}$ device. This is why the $12\text{-}\mu\text{m}$ -core-diameter ARROW VCSEL exhibits multimode operation at a high injection level, while the $8\text{-}\mu\text{m}$ -core-diameter ARROW VCSEL maintains single-mode operation until thermal rollover [4]. However, the high radiation loss of the fundamental transverse leaky mode in the $8\text{-}\mu\text{m}$ device ($\sim 2 \text{ cm}^{-1}$) results in a relatively large threshold current, which is in good agreement with the observation reported in [4].

It must be noted that the value of d_2 used in Fig. 8(a) is obtained from the planar approximation, while that used in Fig. 4 is calculated from our more exact design model [5]. Hence, the value of d_2 given in Fig. 8(a) is not really optimized for the devices.

C. Turn-On Transient Response of ARROW VCSELs

Fig. 9 plots the turn-on transient response of a $12\text{-}\mu\text{m}$ -core-diameter ARROW VCSEL (with $s = 2.4 \mu\text{m}$, $d_2 = 6 \mu\text{m}$, and $\Delta n_b = 0.05$). The laser starts at zero bias and is modulated with a step current density with a magnitude of $\sim 3 \times$ threshold. The

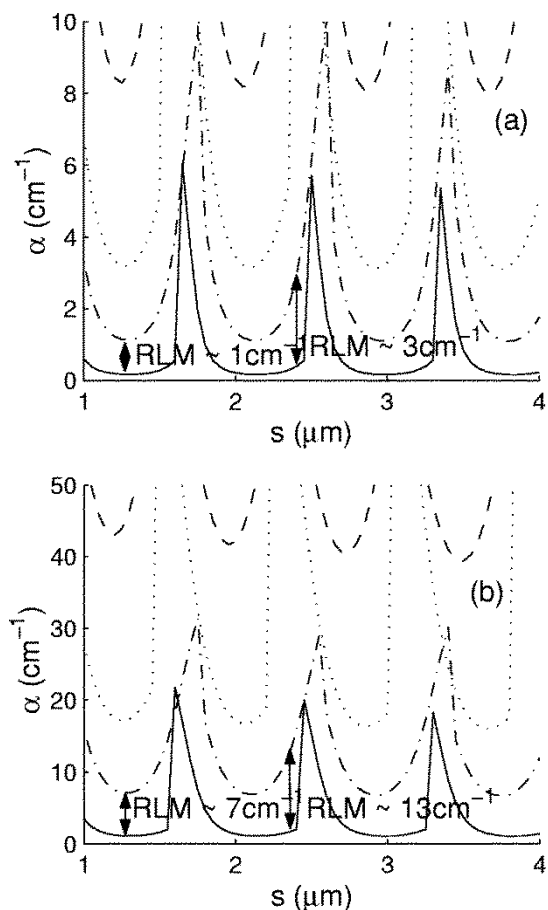


Fig. 8. Radiation loss of the four lowest loss leaky modes plotted against s , with (a) $d_1 = 12 \mu\text{m}$ and $d_2 = 6 \mu\text{m}$ and (b) $d_1 = 8 \mu\text{m}$ and $d_2 = 4 \mu\text{m}$.

influence of the thermal effect is ignored because the thermal lifetime of lasers is much longer than the oscillation period of photon density and carrier concentration. It is observed from Fig. 9(d) that during the first transient period of 0.6 ns, N_{c0} builds up to about $2.3 \times 10^{18} \text{ cm}^{-3}$ inside the core region, thereby exciting the fundamental transverse leaky mode due to the increase in modal gain. However, the excitation of fundamental transverse leaky mode causes SHB of carrier concentration at the center of the core region. It is observed that SHB is established at ~ 0.9 ns, and the first-order transverse leaky mode is excited at around 1.6 ns. As shown in Fig. 9(a), the two transverse leaky modes exhibit antiphase oscillation from 1.6 ns onwards. This antiphase oscillation of fundamental and first-order transverse leaky modes is due to the gain-sharing mechanism inside the core region. The phenomenon of antiphase oscillation is also observed in index-guided VCSELS with a large core diameter [10]. However, the prolonged delay in the excitation of the first-order transverse mode is unique in ARROW VCSELS.

It must be noted that the radiation losses of the transverse leaky modes in ARROW VCSELS are affected by the SHB of carrier concentration. Before 0.8 ns, the corresponding radiation loss of the first-order transverse leaky mode is greater than 23 cm^{-1} (instead of $\sim 3.4 \text{ cm}^{-1}$ obtained from cold-cavity simulation). This is because the high carrier concentration inside the core region significantly reduces the refractive index of the core region of the ARROW structure. Between 0.8 and

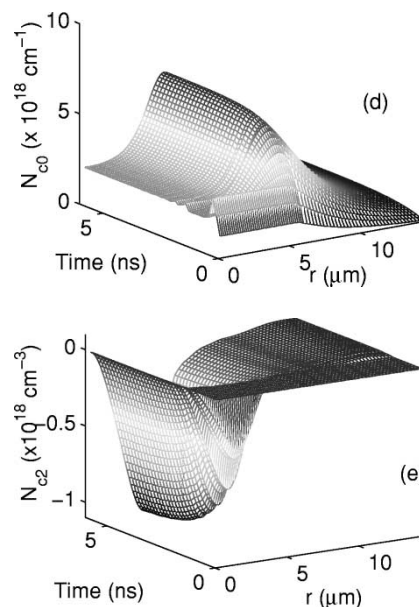
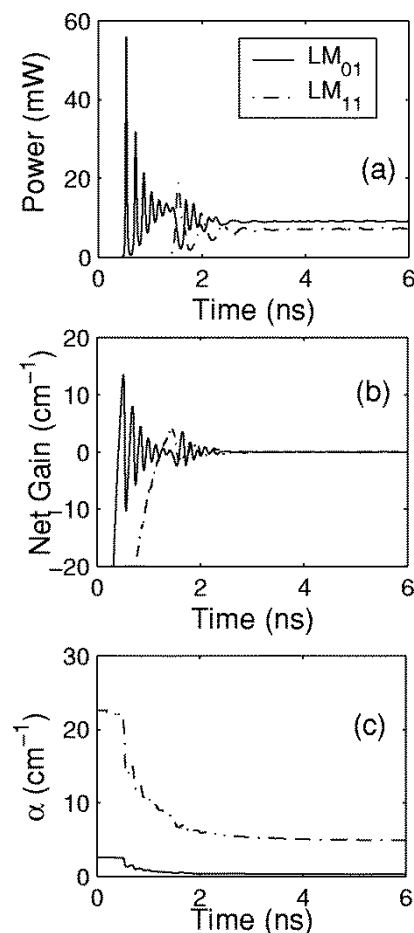


Fig. 9. Turn-on transient response of (a) output power, (b) net modal gain, (c) radiation losses, (d) N_{c0} , and (e) N_{c2} . The solid and dotted-dashed lines represent the fundamental and first-order transverse leaky modes, respectively.

1.6 ns, the SHB of carrier concentration is established, causing the reduction of radiation loss of the first-order transverse leaky mode. Therefore, the corresponding net gain of the first-order transverse leaky mode, defined as $\sum_{i=c,s} (\langle g_{11}^i \rangle - \alpha_{11}^i - \zeta_{11}^i)$, increases from less than -20 to 0 cm^{-1} , enabling it to acquire

threshold. However, it is noted from Fig. 9(c) that the radiation loss of the first-order transverse leaky mode takes a longer time to reach steady state than that of the fundamental transverse leaky mode. Therefore, a prolonged delay in the excitation of the first-order transverse leaky mode is observed in ARROW VCSELs. It should be noted that this phenomenon will not occur in gain- or index-guided VCSEL's because the transverse modes in these devices have no radiation losses.

IV. DISCUSSION AND CONCLUSION

Using the above-threshold model, the steady-state characteristics of 8- and 12- μm -core-diameter ARROW VCSELs are investigated and compared with the experimental results [4]. It is shown that the reason for 8- μm ARROW VCSELs to exhibit better suppression of high-order transverse leaky modes than that of a 12- μm device (under the influence of SHB and thermal lensing effects) is the large RLM. The RLM values of 12- and 8- μm ARROW VCSELs obtained from the cold-cavity simulation [5] are ~ 3 and $\sim 13 \text{ cm}^{-1}$, respectively. This indicated that the possible method for maintaining single-mode operation in ARROW VCSELs is to increase the value of RLM by compromising with a slightly higher threshold current.

In conclusion, the above-threshold characteristics of ARROW VCSELs are studied by a simple self-consistent model, in which the nonuniform distribution of the carrier concentration, optical field intensity and heat are taken into consideration. It is shown that the excitation of high-order transverse leaky modes in ARROW VCSELs under CW operation is mainly dependent on thermal lensing effects. For the lasers under pulsed operation, the SHB of carrier concentration is the only cause of the excitation of high-order transverse leaky modes. A new design rule is also proposed to obtain the optimum dimension of ARROW VCSELs for better suppression of high-order transverse modes. It can be shown that the new optimum dimension of ARROW has significant improvement in SMSR, and the maximum single-mode power can be improved by more than 75%. The turn-on transient response of ARROW VCSELs is also studied. It is shown that the prolonged delay of the excitation of first-order transverse leaky mode is due to the influence of radiation loss.

REFERENCES

- [1] L. J. Mawst, D. Botez, C. Zmudzinski, and C. Tu, "Antiresonant reflecting optical waveguide-type, single-mode diode lasers," *Appl. Phys. Lett.*, vol. 61, pp. 503–505, 1992.
- [2] D. Zhou and L. J. Mawst, "Simplified-antiresonant reflecting optical waveguide-type vertical-cavity surface-emitting lasers," *Appl. Phys. Lett.*, vol. 76, p. 1659, 2000.

- [3] T. W. Lee, S. C. Hagness, D. Zhou, and L. J. Mawst, "Modal characteristics of ARROW-type vertical cavity surface emitting lasers," *IEEE Photon. Technol. Lett.*, vol. 13, pp. 770–772, Aug. 2001.
- [4] D. Zhou and L. J. Mawst, "High-power single-mode antiresonant reflecting optical waveguide-type vertical-cavity surface-emitting lasers," *IEEE J. Quantum Electron.*, vol. 38, pp. 1599–1606, Dec. 2002.
- [5] C. W. Tee and S. F. Yu, "Design and analysis of cylindrical antiresonant reflecting optical waveguide," *J. Lightwave Technol.*, vol. 21, pp. 3379–3386, Dec. 2003.
- [6] L. J. Mawst, D. Botez, R. F. Nabiev, and C. Zmudzinski, "Above-threshold behavior of high-power, single-mode antiresonant reflecting optical waveguide diode lasers," *Appl. Phys. Lett.*, vol. 66, no. 1, pp. 7–9, Jan. 1995.
- [7] J. C. Chang, J. J. Lee, A. Al-Muhanna, L. J. Mawst, and D. Botez, "Comprehensive above-threshold analysis of large-aperture (8–10 μm) antiresonant reflecting optical waveguide diode lasers," *Appl. Phys. Lett.*, vol. 81, no. 26, pp. 4901–4903, Dec. 2002.
- [8] K. H. Hahn, M. R. Tan, Y. M. Houg, and S. Y. Wang, "Large area multitransverse mode VCSEL's for modal noise reduction in multimode fiber systems," *Electron. Lett.*, vol. 29, no. 6, pp. 1482–1283, 1993.
- [9] Y. G. Zhao and J. G. McInerney, "Transverse mode control of vertical cavity surface emitting lasers," *IEEE J. Quantum Electron.*, vol. 32, pp. 1950–1958, Nov. 1996.
- [10] A. Valle, "Selection and modulation of high-order transverse modes in vertical cavity surface emitting lasers," *IEEE J. Quantum Electron.*, vol. 34, pp. 1924–1932, Oct. 1998.
- [11] C. W. Tee, C. C. Tan, and S. F. Yu, "Design of antiresonant reflecting optical waveguide-type vertical cavity surface emitting lasers using transfer matrix method," *IEEE Photon. Technol. Lett.*, vol. 15, pp. 1231–1233, Sept. 2003.
- [12] S. F. Yu and E. H. Li, "Effects of lateral modes on the static and dynamic behavior of buried heterostructure DFB lasers," *Proc. Inst. Elect. Eng.—Optoelectronics*, vol. 142, no. 2, pp. 97–102, 1995.
- [13] S. F. Yu, "Polarization bistability in vertical cavity surface emitting semiconductor lasers," *J. Lightwave Technol.*, vol. 15, pp. 1032–1041, June 1997.
- [14] M. S. Miguel, Q. Feng, and J. V. Moloney, "Light-polarization dynamics in surface-emitting semiconductor lasers," *Phys. Rev. A, Gen. Phys.*, vol. 52, no. 2, pp. 1728–1739, 1995.
- [15] N. K. Dutta, "Analysis of current spreading, carrier diffusion, and transverse mode guiding in surface emitting lasers," *J. Appl. Phys.*, vol. 68, pp. 1961–1963, 1990.
- [16] Y. G. Zhao and J. G. McInerney, "Transient temperature response of vertical-cavity surface-emitting semiconductor lasers," *IEEE J. Quantum Electron.*, vol. 31, pp. 1668–1673, Sept. 1995.
- [17] S. F. Yu, "Polarization selection in birefringent antiresonant reflecting optical waveguide-type vertical cavity surface emitting lasers," *IEEE J. Quantum Electron.*, vol. 39, pp. 1362–1371, Nov. 2003.

C. W. Tee (S'04), photograph and biography not available at the time of publication.

S. F. Yu (SM'03), photograph and biography not available at the time of publication.

N. S. Chen, photograph and biography not available at the time of publication.